A Convex Optimization Approach to Solar Sail Station-Keeping Control in Halo Orbits

Fausto Vega
The Robotics Institute
Carnegie Mellon University
Pittsburgh, PA 15213
fvega@andrew.cmu.edu

Zachary Manchester
The Robotics Institute
Carnegie Mellon University
Pittsburgh, PA 15213
zacm@cmu.edu

***Abstract*— We present a convex optimization-based station-keeping control algorithm designed for long-term station keeping of unstable halo orbits using a solar sail. Our controller determines a sail orientation to minimize deviations from a nominal halo orbit. Traditional methods often linearize the solar-sail propulsion model around nominal angles that define the sail orientation, but this can lead to inaccuracies as the model deviates from the linearization point. Instead, we encode the set of possible thrust vectors generated by the nonlinear solar sail model as the boundary of a convex set, which we then relax to arrive at a convex optimization problem. We demonstrate empirically that this relaxation is tight in most cases (i.e. it produces feasible solutions to the original problem) in realistic simulation examples in the Earth-Moon system, validating the effectiveness of this propulsion-free method for long-term station keeping.**

TABLE OF CONTENTS

1. INTRODUCTION

Halo-orbit missions enable efficient exploration and continuous visibility of a celestial body's surface. Despite their instability, they require minimal delta-v for station keeping. These characteristics make halo orbits ideal locations for positioning, navigation, and timing (PNT) systems [1]. In addition, they are suitable for space stations aimed at extending human presence to cislunar space [2], an area of growing interest to NASA. The thrust required to track these orbits is typically provided using chemical propulsion. However, these propulsion systems have notable drawbacks: they increase the spacecraft's mass because of the fuel onboard and limit the mission duration based on the available propellant. The CAPSTONE mission, the first CubeSat to operate in cislunar space, exemplifies these limitations [3]. It employs a monopropellant hydrazine propulsion system that provides a delta-v budget of 200 m/s, restricting the mission duration to approximately two years [4].

979-8-3503-5597-0/25/$31.00 ©2025 IEEE

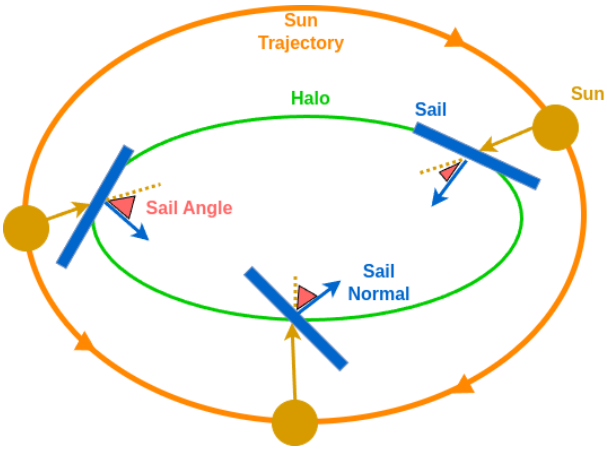

Figure 1: This conceptual illustration depicts three simplified solar-sail orientations in the rotating circular-restricted three-body problem frame, demonstrating how a solar sails can track an unstable halo orbit by changing it's attitude with respect to the incident sun direction. Our algorithm determines the sail normal vector to effectively track a halo orbit for long-term station keeping.

Solar sailing, in contrast, exploits the limitless delta-v provided by solar radiation pressure. The sail generates thrust through the impact of photons emitted by the Sun onto its reflective surface [5], enabling long-term missions. Currently, solar-sail missions have primarily been technology demonstrations. Examples include JAXA's Interplanetary Kite-craft Accelerated by Radiation Of the Sun (IKAROS) mission [6], which successfully deployed a 196 m^2 sail in 2010, and The Planetary Society's LightSail 2 mission, which deployed a 32 m^2 sail to provide on-orbit validation of sail deployment and control in low-earth orbit [7].

The LightSail 2 mission implemented a control strategy that involved reorienting the sail twice per orbit to raise its apogee [8]. While this on-off strategy proved successful for Earth-orbiting missions, it may not be effective in halo orbits because of the chaotic dynamics present in three-body regimes. Stationkeeping for halo orbits using a solar sail has been studied in simulation: Farres [9] applied a dynamical systems approach, calculating the sail angle needed to return the spacecraft to its trajectory using stable invariant manifolds when it reaches some maximum deviation. Bookless derived an optimal control law in closed form for both area and angle control of the sail to maintain a Lissajous orbit L2 [10]. However, both techniques rely on linearizing about two angles that parameterize the sail normal vector direction, which limits performance and can lead to inaccuracies as the model deviates from the linearization point.

In this paper, we develop a convex-optimization approach to the solar sail halo-orbit station-keeping control problem that avoids linearization about some reference orientation, enabling higher performance and robustness to larger disturbances and injection errors. To address the nonlinear solar-sail propulsion model, we encode the feasible set of possible thrust vectors generated by the sail as the boundary of a convex set, avoiding the small-angle approximations used in prior works. We approximate this convex set as an ellipsoid, enabling use of efficient second-order cone program (SOCP) solvers [11] [12]. As an optional "solution-polishing" step, we can then project the approximate solution generated by the SOCP solver onto the exact thrust manifold. We employ this algorithm in a receding-horizon scheme to successfully track an unstable halo orbit in the Earth-Moon system in simulation.

Our contributions include:

1. A convex formulation of the nonlinear solar-sail propulsion constraint, and an approximation of this constraint as an ellipsoid.
2. A receeding-horizon controller that computes the sail's normal vector to stabilize and track an unstable halo orbit.
3. Simulation results in the Earth-Moon system demonstrating the effectiveness of our approach.

The remainder of the paper is organized as as follows: In Section 2, we introduce the circular restricted three-body problem (CR3BP) along with the solar-sail propulsion model used in our analysis. Next, we derive our trajectory optimization formulation and a receding-horizon control strategy in Section 3. Then, we present our closed-loop simulation results in Section 4. Finally, we summarize our conclusions and directions for future work in Section 5.

2. BACKGROUND

This section provides a brief review of the CR3BP along with the solar-sail propulsion model used in our analysis. We refer interested readers to [13] and [5] for more detailed treatments.

The Circular Restricted Three-Body Problem

The CR3BP models the motion of a small third body under the gravitational influence of two larger primary bodies. This framework assumes that the two primary masses, m_1 and m_2, orbit their common barycenter in circular paths, with m_1 being larger than m_2. The third body is considered to have infinitesimal mass. To enhance numerical stability, the system is normalized: the combined mass of the primaries is set to unity, the distance between m_1 and m_2 is defined as 1, and their rotation rate about the barycenter is also normalized to unity. We use a rotating frame about the barycenter so that the two primary masses are fixed on the x-axis of the rotating frame. In this work, we performed all the analysis in the Earth-Moon system.

We extend the CR3BP equations by incorporating the effect of solar radiation pressure on the sail, represented by the force vector $u = [u_x, u_y, u_z]$. The state of the spacecraft x consists of its position $q = [q_x, q_y, q_z]$ and velocity $v = [v_x, v_y, v_z]$ in nondimensionalized units. The controlled continuous CR3BP equations of motion $\dot{x} = f(x,u)$ that describe the state of the spacecraft in the rotating frame are given by (1),

$$\begin{aligned}
\dot{q}_x &= v_x \\
\dot{q}_y &= v_y \\
\dot{q}_z &= v_z \\
\dot{v}_x &= \frac{\partial U}{\partial q_x} + 2v_y + \frac{u_x}{m} \\
\dot{v}_y &= \frac{\partial U}{\partial q_y} - 2v_x + \frac{u_y}{m} \\
\dot{v}_z &= \frac{\partial U}{\partial q_z} + \frac{u_z}{m}
\end{aligned} \tag{1}$$

where U is the augmented potential expressed in (2), μ is the characteristic mass parameter of the CR3BP, and m is the mass of the spacecraft. For the Earth-Moon system the mass parameter is $\mu = 1.215058560962404 \times 10^{-2}$.

$$\begin{aligned}
U &= \frac{1}{2}(q_x^2 + q_y^2) + \frac{1-\mu}{r_1} + \frac{\mu}{r_2} \\
r_1 &= [(q_x+\mu)^2 + q_y^2 + q_z^2]^{\frac{1}{2}} \\
r_2 &= [(q_x-1+\mu)^2 + q_y^2 + q_z^2]^{\frac{1}{2}}
\end{aligned} \tag{2}$$

To obtain a discrete-time dynamics model $x_{k+1} = f_d(x_k, u_k)$, we apply a fourth-order Runge-Kutta integrator to the continuous dynamics in (1). This model provides the next state of the spacecraft x_{k+1} given a state x_k and a control u_k at the time step k. The control input u_k is discretized using a zero-order hold.

Solar Sail Propulsion Model

A solar sail generates thrust through the impact of photons emitted by the Sun onto its reflective surface [5]. We assume a perfectly reflecting sail, implying that the force vector u aligns with the sail normal n. The incident sun direction is represented by s while α represents the angle between the sail normal and the incident sun direction, as illustrated in Figure 2.

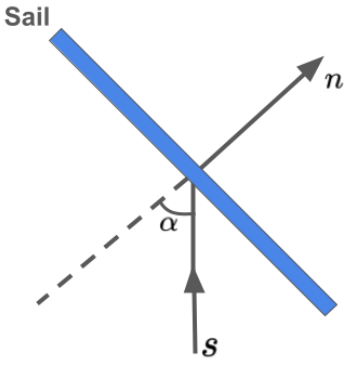

Figure 2: Solar sail model notation

The nonlinear solar-sail thrust model is:

$$u = \gamma(s^T n)^2 n. \tag{3}$$

This model demonstrates that the force produced by the sail is dependent on the sail attitude, which is represented by the sail

normal vector n. The parameter γ in (3) denotes the maximum thrust magnitude achievable when the sail normal is aligned with the incident sun direction.

The maximum thrust magnitude is given by,

$$\gamma = \frac{2A}{c} W_E \left(\frac{R_E}{r} \right)^2, \tag{4}$$

where A is the sail area, c is the speed of light, W is the solar radiation intensity (assumed to be 1368 W/m^2 at 1 AU), R_E is the Earth-Sun distance, and r is the distance between the sun and the spacecraft.

Plotting all the possible thrust vectors that the sail can generate, as described by (2), results in a nearly ellipsoidal 3D surface. Figure 3 illustrates a 2D cross section of this 3D control set in the y-z-plane, assuming that the incident sun direction is aligned with the z-axis and a sail area of 10 m^2. The maximum acceleration this sail can produce is approximately 9.126×10^{-5} m/s^2.

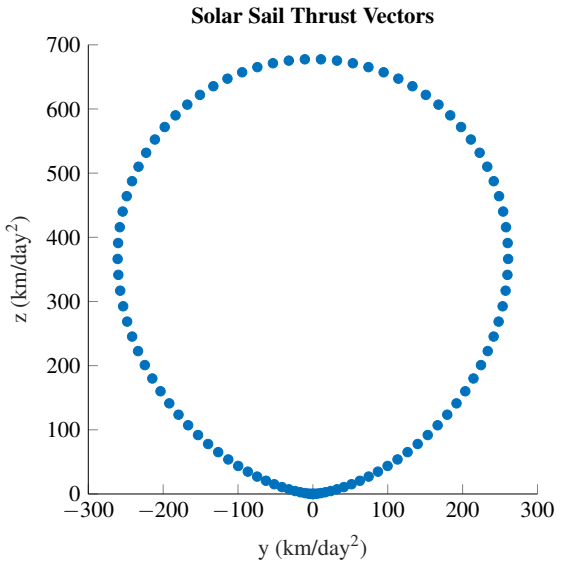

Figure 3: Thrust vectors generated by a 10 m^2 sail.

3. Optimization-Based Solar Sailing

This section presents our trajectory optimization formulation for determining solar-sail attitudes for station keeping around an unstable halo orbit in the Earth-Moon system.

Reference Trajectory and Linearized Dynamics

Using the CR3BP, we formulate a periodic halo orbit around the L2 Lagrange point as our reference trajectory. This orbit has a period of 14.81 days and exhibits instability. Specifically, it has a x-amplitude of 23,354 *km*, y-amplitude of 67,591 *km*, and z-amplitude of 5,422 *km*. Without active control, a spacecraft on this trajectory would deviate significantly after only one revolution. Figure 4 illustrates the reference halo trajectory.

We then discretize the reference halo orbit into N knot points and linearize our dynamics about each knot point $\bar{x}_k$ using a first-order Taylor expansion. This linearization allows us to

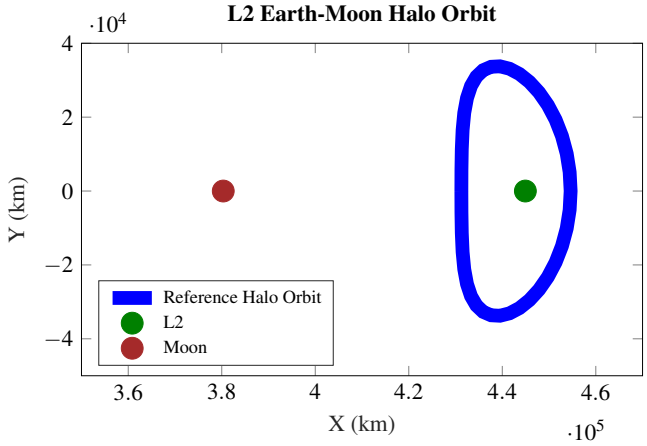

Figure 4: Halo orbit around the L2 Lagrange point in the Earth-Moon barycentric rotating frame

represent the dynamics as a linear equality constraint, which is required to formulate a convex optimization problem. The resulting linear dynamics can be expressed as:

$$\begin{aligned} \Delta x_{k+1} &\approx A_k \Delta x_k + B_k u_k \\ A_k &= \left. \frac{\partial f_d}{\partial x_k} \right|_{(\bar{x}_k, u_k)} \\ B_k &= \left. \frac{\partial f_d}{\partial u_k} \right|_{(\bar{x}_k, u_k)} \\ \Delta x_k &= x_k - \bar{x}_k \end{aligned} \tag{5}$$

where A_k and B_k are the discrete dynamics Jacobians evaluated at each knot point $\bar{x}_k$ along the reference trajectory. We note that, in contrast to prior approaches that linearize the sail attitude about some reference angles, our approach only linearizes the CR3BP dynamics in the neighborhood of the reference halo orbit, while still capturing the full range of possible sail orientations.

Solar Sail Control Set Approximation

To simplify the parameterization of the 3D solar sail control set, we approximate it as an ellipsoid. In two dimensions, this approximation is equivalent to fitting an ellipse to the projection of the true control set. The symmetry of the true control set in two axes simplifies our analysis because we only need to solve for two axis lengths. We formulate this as a least-squares optimization problem to find the parameters of a 2D ellipse that best fits the projected control set in Figure (3). The problem is expressed in (6):

$$\begin{aligned} &\min_{a,b,y_c,z_c} \quad \frac{1}{N_k} \sum_{k=1}^{N} e_k^2 \\ &e_k = \frac{(y_k - y_c)^2}{a^2} + \frac{(z_k - z_c)^2}{b^2} - 1 \end{aligned} \tag{6}$$

where e_k is the residual function, (y_c, z_c) represents the ellipse center, N_k is the number of samples on the control set, and a and b are the semi-major and semi-minor axes lengths, respectively. We solve the optimization problem using Newton's method, resulting in the approximation shown in Figure 5. The length of the major axis $2a$ corresponds to γ from

(4). We denote the length of the other two symmetric axes as β, which is equivalent to $2b$. This approximation provides a simplified, yet sufficiently accurate representation of the true solar sail control set, facilitating the convex formulation of the trajectory-tracking problem.

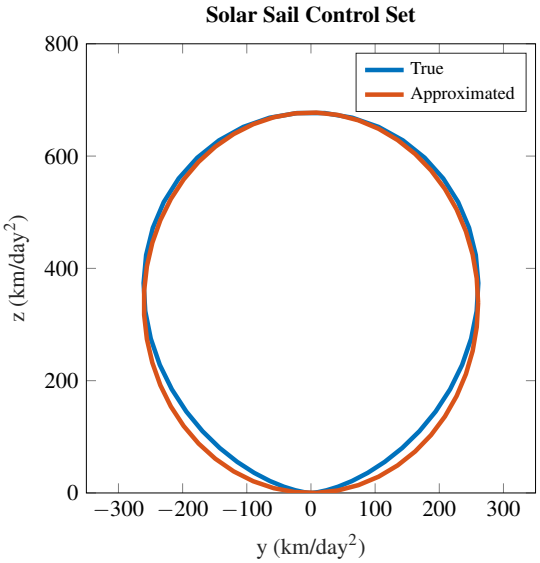

Figure 5: True control set and approximated control set via least squares optimization of the solar sail model. The length of the major axis is γ and the length of the minor axis is β.

We assume that the parameters of this ellipse are constant throughout the whole mission as the change in γ is minimal.

Optimization-Based Station keeping

We formulate the solar sail station-keeping problem as the following trajectory optimization problems:

$$\begin{aligned} \underset{x_{1:2N},u_{1:2N-1}}{\text{minimize}} \quad & J = \sum_{k}^{2N-1} l_k(x_k,u_k) + l_N(x_k) \\ \text{subject to} \quad & g(x_k,u_k) = 0 \\ & h(x_k,u_k) \leq 0 \end{aligned} \tag{7}$$

In this formulation, $l_k(x_k,u_k)$ represents the stage cost, $l_N(x_k,u_k)$ denotes the terminal cost, while $g(x_k,u_k)$ and $h(x_k,u_k)$ define the equality and inequality constraints, respectively. The parameter N represents the number of discrete knot points over one period of the orbit. For a convex optimization problem, the equality constraints are required to be affine, and both the cost function and the inequality constraints must be convex functions [14]. This combination of conditions guarantees that a globally optimal solution to the problem can be found efficiently (e.g. with an interior-point method).

We solve over a two-orbit horizon and constrain the thrust vector to the boundary of the ellipsoid approximation. Since the ellipsoid boundary is a nonconvex set, we relax this constraint with an inequality to include the interior of the ellipsoid. This approach allows us to maintain convexity in our optimization problem at the expense of possibly introducing infeasible thrust vectors. These infeasible thrust vectors correspond to solutions in the interior of the ellipsoid.

The ellipsoid is represented in matrix form as the quadratic inequality $x^T P x \leq 1$. For each timestep k, we derive the ellipsoid matrix P_k as a function of two key elements: the incident sun direction s_k and the axis lengths (γ and β) obtained from the least-squares fit of the 2D ellipse. Equation (8) presents this formulation, with its detailed derivation provided in the Appendix:

$$P_k(\gamma,\beta,s_k) = \frac{4}{\beta^2} + 4\left(\frac{1}{\gamma^2} - \frac{1}{\beta^2}\right) s_k s_k^T \tag{8}$$

To promote solutions that lie on the ellipsoid's boundary, we implement a one-norm cost $l_k(x) = \|\Delta x\|_1$ on state deviations. This approach encourages the generation of "bang-bang" thrust vectors [15], which tend to push toward the boundary of the ellipsoid.

The full convex problem formulation is:

$$\begin{aligned} \min_{\Delta x_{1:2N},\Delta u_{1:N-1}} \quad & \sum_{k=1}^{2N} \|\Delta x_k\|_1 \\ \text{s.t.} \quad & \Delta x_{k+1} = A_k \Delta x_k + B_k \Delta u_k \\ & \Delta x_k^T P_k \Delta x_k - 1 \leq 0 \\ & -\Delta u_k^T s_k \leq 0 \end{aligned} \tag{9}$$

The first constraint corresponds to the linear state-error dynamics form (5), the second constraint is the relaxed ellipsoid constraint parameterized by (8), and the third constraint ensures the control is in the direction of the incident sun direction. Solving (9) results in an optimal solution for the approximated control set (ellipsoid); however, it may not be dynamically feasible due to the control set approximation not being exact as seen in Figure 5. To address this, we implement a second-stage projection step, in which we project the solution from (9) onto the true solar sail control set defined by (3). This second stage is a non-convex least squares optimization problem. However, since the ellipsoid solution closely approximates the true constraint, the first-stage solution provides a very good initial guess and this stage typically converges very quickly in a few iterations.

The second-stage projection problem problem is,

$$\begin{aligned} \min_{\Delta u_{c_{1:N-1}},n_{1:N-1}} \quad & \sum_{k=1}^{N-1} ||\Delta u_k - \Delta u_c||^2 \\ \text{s.t.} \quad & \gamma(s_k^T n_k)^2 n_k - \Delta u_k = 0 \\ & n_k^T n_k - 1 = 0 \\ & -s_k^T n_k \leq 0 \end{aligned} \tag{10}$$

where Δu_k is the solution from the first stage convex problem and Δu_c and n are the decision variables for the control and normal vector on the true constraint set. The first constraint represents the true solar sail control set as defined in (3). The second constraint ensures the normal vector maintains unit length, while the third constraint guarantees that the normal vector points toward the incident sun direction.

We implement this two-stage optimization procedure as a receding-horizon or model-predictive controller (MPC). In this approach, we solve problems (9) and (10), then apply only the first control to the nonlinear CR3BP dynamics. This

process is then repeated at each time step to compensate for disturbances and model errors based on the most recent state information.

The complete solar sail MPC procedure is summarized in Algorithm 1.

Algorithm 1 Solar Sail Model MPC Algorithm

```
Initialize model, constraints, and prediction horizon 2N
Set initial state x_0 with injection error
while k = 1:2N do
    Estimate current state x_k
    Solve convex optimization problem (9)
    Solve nonconvex optimization problem (10)
    Simulate the first control input u_c of (10) to the nonlinear CR3BP discrete dynamics model
    k ← k + 1
end while
```

4. Simulation Experiments

We conduct our simulations in the Earth-Moon CR3BP system. Our focus is on tracking an unstable periodic orbit around the L2 Lagrange point, as illustrated in Figure 4. This particular orbit has a period of 14.81 days. For our spacecraft model, we assume a 3U CubeSat with a mass of 4 kg equipped with a 10 m^2 solar sail. All simulation code is available on Github[2].

First, we discretize the L2 Earth-Moon halo into 81 knot points (N) which results in a timestep $\Delta t = 4.4556$ hours. Then, we obtain the trajectory of the Sun in the Earth-centered inertial frame through JPL ephemeris data using Spice.jl [16], and convert it into the CR3BP rotating frame. For our simulations, the initial epoch was set arbitrarily to December 20, 2018.

The optimization problem is then formulated using Convex.jl [17], a convex optimization modeling framework in Julia [18]. We then solve the convex problem using the Clarabel solver [19] to tight tolerances. The second-stage correction step is solved using IPOPT [20]. To simulate nonlinear CR3BP dynamics, we utilize a high-order Runge-Kutta method, specifically the Tsitouras-Papakostas 8/7 Runge-Kutta method in DifferentialEquations.jl [21].

Earth-Moon Simulation

The injection error corresponds to the initial deviation (Δx) from the halo initial condition. For this simulation, we set the injection error to 385.5 meters in each direction, and 18.5 cm/s in each velocity direction. The algorithm is able to successfully track a 100-revolution (3.8 year) trajectory; however, we present the initial 3-revolution trajectory as it shows the control maneuver the satellite executes to resolve the initial injection error. Each revolution consists of 80 convex solves. Over the course of the 100-revolution trajectory, 98% of the solutions status indicate optimality, while the remaining 2% exceed the user-specified iteration limit. However, the algorithm remains feasible at every timestep, as the control is always projected on the true control set, and the forward simulation uses the true nonlinear dynamics. Figure 6 shows the trajectory of the solar sail angle and the thrust magnitude generated by the sail for the first three revolutions.

[2]https://github.com/RoboticExplorationLab/cvx-mpc-solarsailing

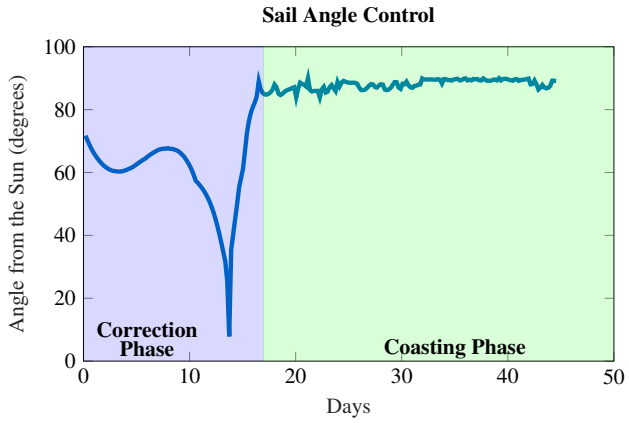

(a) Solar sail angle from the incident sun vector to complete three revolutions around an unstable L2 halo orbit in the Earth-Moon system.

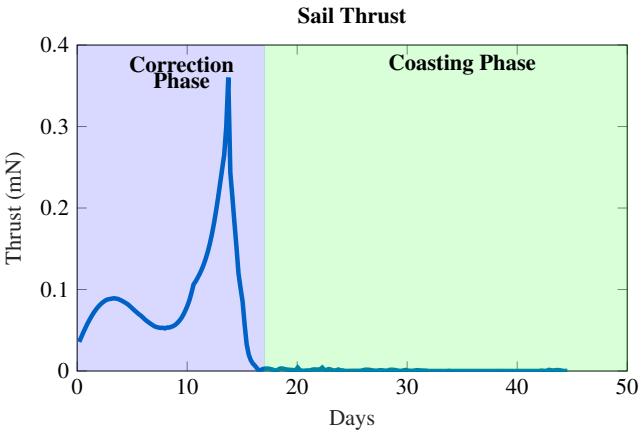

(b) Velocity deviation from the L2 halo orbit for three revolutions.

Figure 6: Solar sail angle and thrust magnitude for station-keeping around an unstable L2 halo orbit in the Earth-Moon system. The larger the angle from the incident sun direction leads to a smaller thrust magnitude.

The solution is divided into two phases, the correction phase and the coasting phase. The correction phase corrects for the initial injection error from the halo orbit, and the satellite is able to do this within the first revolution. The satellite applies a large maneuver on day 14 because the state deviation is aligned with the sun position at this time. Once the satellite reaches the halo ($\Delta x = 0$), it only needs minor corrections due to the instability of the orbit and primarily uses the dynamics to complete its revolutions. We assume that there is no eclipse during the correction phase. However, if there is an eclipse during the coasting phase, the satellite would still be able to track the halo because not much thrust is needed.

The solar sail thrust vector exhibits a large change in thrust during the correction phase. However, since the timesteps are several hours, the spacecraft should have sufficient time to adjust it's attitude within each time window. Specifically, the highest angular rate is 1.8×10^{-3} deg/s throughout the three-revolution trajectory in Fig. 6a, which is achievable with a reaction wheel attitude control system onboard the Cubesat [22]. One approach to reduce oscillation is to add a cost on the time derivative of the control, however, this leads to solutions in the interior of the ellipsoid which are

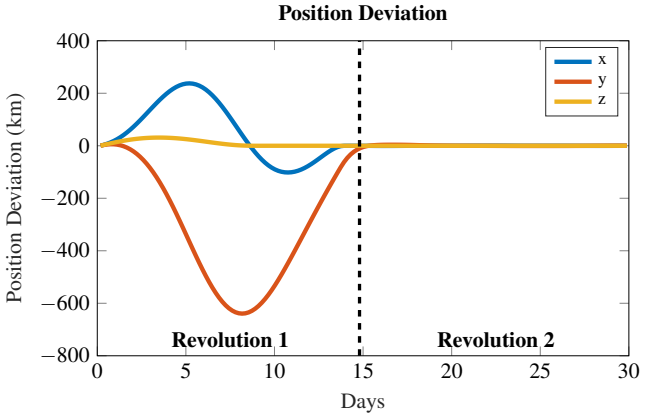

(a) Position deviation from the L2 halo orbit for two revolutions.

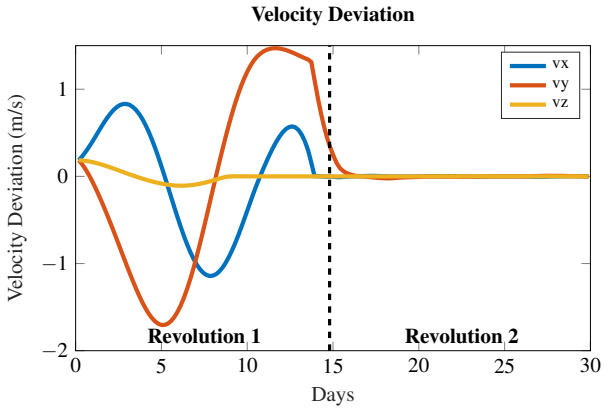

(b) Velocity deviation from the L2 halo orbit for two revolutions.

Figure 7: State deviation from the L2 halo orbit in the Earth-Mon system. The dashed line represents the end of the first revolution.

suboptimal. Figure 7 illustrates the state deviation from the reference halo orbit trajectory which converges to zero after the first revolution.

The second stage projection modifies the optimal solution obtained from the convex problem, but the magnitude of this change is typically small. In the three-revolution example, the solution to the convex problem (9) always remained on the boundary of the ellipsoid, and the differences between the ellipsoid approximation and true control set are quite small (Fig. 5). We plot the magnitude of the change of the convex approximated solution to the projected true solution over one revolution in Fig. 8. These relatively small adjustments indicate that the ellipsoid solutions closely approximate the true control set. While not strictly optimal, our algorithm produces suboptimal solutions that provide sail thrust vectors capable of stabilizing and tracking an unstable halo orbit for extended periods using only solar radiation pressure.

We provide an additional example using a different periodic orbit around L2 in the Appendix.

Monte Carlo Simulation

We conducted a Monte Carlo simulation by generating 100 injection errors sampled from a Gaussian distribution. This distribution has a standard deviation of 385 meters for the position components and 18.5 cm/s for the velocity components.

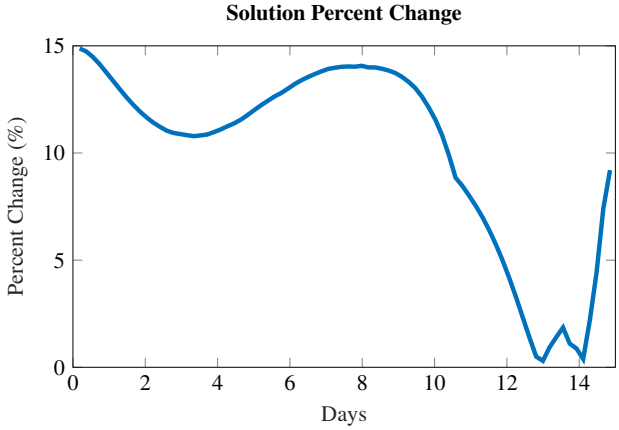

Figure 8: Change in the thrust vector magnitude of the second-stage solution compared to the first-stage thrust vector magnitude for the first revolution.

Each simulation computed a five-revolution trajectory, with the algorithm solving 98% of the cases. Figure 9 illustrates the Euclidean norm of the position and velocity deviations for the successful cases, showing converge to zero after 40 days (approximately 2.5 revolutions). The two failure cases have a high initial velocity deviation of around 29 cm/s in both the x and y directions, causing the satellite to escape the halo orbit trajectory. This escape was caused by insufficient thrust from the sail to correct the trajectory. As a result, there exists a section in the state space where the problem becomes uncontrollable due to unfavorable initial conditions and the Sun's initial position.

5. Conclusions

In this work, we have developed a convex receding-horizon control strategy to stabilize and track halo orbits with a solar sail, and demonstrated the method in numerical simulations in the Earth-Moon system. Our approach utilizes an approximation of the control set to solve a convex optimization problem, followed by a projection step to correct the solution onto the true control set. The effectiveness of this method is demonstrated by its ability to track 100 revolutions of an unstable halo orbit, highlighting its potential for long-term, high delta-v missions.

While solar sailing offers significant advantages, it is important to acknowledge its limitations. These include sail degradation over time and the high risk associated with deployment failure. Despite these challenges, solar sailing CubeSat propulsion in cislunar space could enable a new class of long-duration low-cost scientific and exploration missions.

In future work we plan to eliminate the projection step of our algorithm by expressing the exact control set in a convex manner through semidefinite programming relaxations, as well as applying our method to other halo-orbit and station-keeping scenarios.

Appendices

This section derives the matrix P corresponding to the ellipsoid constraint as a function of the incident sun direction and

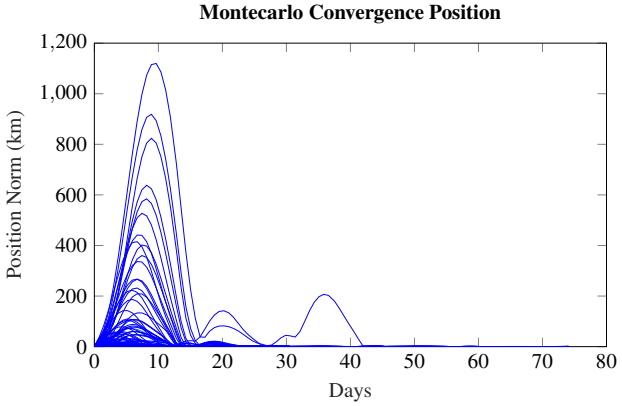

(a) Euclidean norm of the position deviation from the L2 halo orbit for 98 out of 100 Monte Carlo trials.

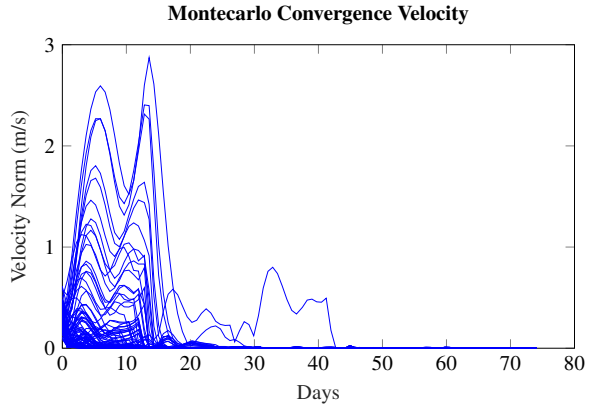

(b) Euclidean norm of the velocity deviation from the L2 halo orbit for 98 out of 100 Monte Carlo trials.

Figure 9: Euclidean norm of the state deviation from the L2 halo orbit in the Earth-Moon system of 98 out of 100 Monte Carlo trials. Each simulation had a period of 5 revolutions.

axes lengths.

A. Ellipsoid Calculation

An ellipsoid is the intersection of a quadratic form as shown in (11) where,

$$x^T P x = 1 \tag{11}$$

$x \in \mathbb{R}^3$ is the state vector and $P \in \mathbb{R}^{3\times3}$ is a symmetric, positive definite matrix containing the information of the ellipsoid. Specifically, the eigenvalues λ of P are inversely related to the squares of the semi-major axes, and the eigenvectors e determine the direction of these axes. We can demonstrate this relation through the eigendecomposition of P.

$$x^T \begin{bmatrix} e_1 & e_2 & e_3 \end{bmatrix} \begin{bmatrix} \lambda_1 & 0 & 0 \\ 0 & \lambda_2 & 0 \\ 0 & 0 & \lambda_3 \end{bmatrix} \begin{bmatrix} e_1^T \\ e_2^T \\ e_3^T \end{bmatrix} x = 1 \tag{12}$$

Expanding this relation results in (13).

$$\lambda_1 x^T e_1 e_1^T x + \lambda_2 x^T e_2 e_2^T x + \lambda_3 x^T e_3 e_3^T x = 1 \tag{13}$$

We can then rewrite (13) in standard form to show the relation between the size of the ellipse and it's eigen decomposition.

$$\frac{(e_1^T x)^2}{\left(\frac{1}{\sqrt{\lambda_1}}\right)^2} + \frac{(e_2^T x)^2}{\left(\frac{1}{\sqrt{\lambda_2}}\right)^2} + \frac{(e_3^T x)^2}{\left(\frac{1}{\sqrt{\lambda_3}}\right)^2} = 1 \tag{14}$$

Since we know the length of the major and minor axes are γ and β from the least squares analysis, we can solve for the eigenvalues of P as shown in (15).

$$\begin{aligned} \lambda_1 &= \frac{4}{\gamma^2} \\ \lambda_2 &= \frac{4}{\beta^2} \\ \lambda_3 &= \frac{4}{\beta^2} \end{aligned} \tag{15}$$

Factoring (13), we see that P is made up of the sum of three rank one matrices.

$$x^T(\lambda_1 e_1^T e_1 + \lambda_2 e_2^T e_2 + \lambda_3 e_3^T e_3)x = 1 \tag{16}$$

Eigenvector e_1 is always pointed toward the incident sun direction s and the sum of the rank one matrices corresponding to e_2 and e_3 can be calculated as a function of e_1 by calculating the orthogonal subspace of e_1 through a projection.

$$x^T(\lambda_1 e_1^T e_1 + \lambda_2(I - e_1 e_1^T))x = 1 \tag{17}$$

Substituting all the variables derives the equation of the ellipsoid shown in (8) as a function of the incident sun direction.

$$P(\gamma, \beta, s) = \frac{4}{\beta^2} + 4\left(\frac{1}{\gamma^2} - \frac{1}{\beta^2}\right) ss^T \tag{18}$$

B. Additional Example

We ran the algorithm on a different L2 halo orbit in the Earth-Moon system with the same discretization. The orbit initial condition was obtained through the JPL Solar System Dynamics site [23] in normalized units, and the exact initial condition is available on the Github repository. The orbit has a period of 14.29 days and exhibits amplitudes of 36,272 km along the x-axis, 100,931 km along the y-axis, and 82,625 km along the z-axis, as illustrated in Figure 10. We set the injection error to the same values as in the previous example, 385.5 meters and 0.185 m/s in each direction. Figure 11 shows the solar-sail angle and thrust trajectory for a two-revolution period. Similarly to the previous orbit, a large maneuver is required around day 14 to correct the trajectory from the initial injection error followed my minor corrections to correct for the orbit instability. Figure 12 shows the state deviation converging close to zero during the second revolution demonstrating the success of the algorithm for stationkeeping using a 10 m^2 solar sail.

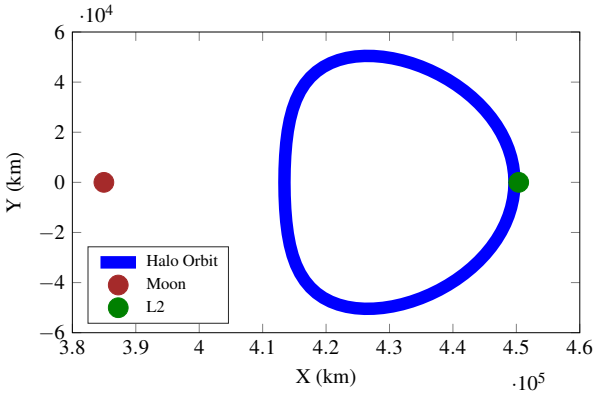

Figure 10: Halo orbit around the L2 Lagrange point in the Earth-Moon barycentric rotating frame for Example 2

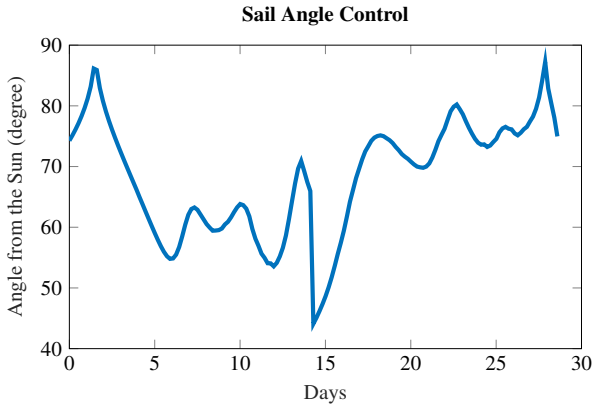

(a) Solar sail angle from the incident sun vector to complete two revolutions around an unstable L2 halo orbit in the Earth-Moon system.

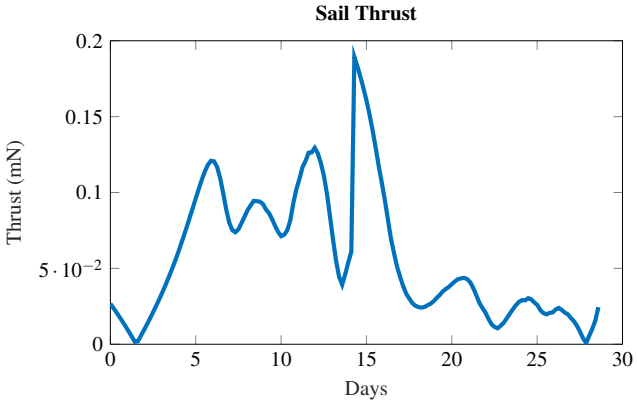

(b) Velocity deviation from the L2 halo orbit for two revolutions.

Figure 11: Solar sail angle and thrust magnitude for station-keeping around an unstable L2 halo orbit in the Earth-Moon system for Example 2.

ACKNOWLEDGMENTS

This work was supported by the National Science Foundation under grant No. DGE2140739 and by the Jet Propulsion Laboratory's Strategic University Research Partnership Program. The authors thank Martin Lo and Jon Arrizabalaga for valuable feedback and discussions on experiment design.

REFERENCES

[1] C. Circi, D. Romagnoli, and F. Fumenti, "Halo orbit dynamics and properties for a lunar global positioning system design," *Monthly Notices of the Royal Astronomical Society*, vol. 442, no. 4, pp. 3511–3527, 2014.

[2] J. Crusan, J. Bleacher, J. Caram, D. Craig, K. Goodliff, N. Herrmann, E. Mahoney, and M. Smith, "Nasa's gateway: An update on progress and plans for extending human presence to cislunar space," in *2019 IEEE Aerospace Conference*. IEEE, 2019, pp. 1–19.

[3] B. Cheetham, "Cislunar autonomous positioning system technology operations and navigation experiment (capstone)," in *ASCEND 2021*, 2021, p. 4128.

[4] T. Gardner, B. Cheetham, A. Forsman, C. Meek, E. Kayser, J. Parker, M. Thompson, T. Latchu, R. Rogers, B. Bryant *et al.*, "Capstone: A cubesat pathfinder for the lunar gateway ecosystem," 2021.

[5] C. R. McInnes, *Solar sailing: technology, dynamics and mission applications*. Springer Science & Business Media, 2004.

[6] Y. Tsuda, O. Mori, R. Funase, H. Sawada, T. Yamamoto, T. Saiki, T. Endo, K. Yonekura, H. Hoshino, and J. Kawaguchi, "Achievement of ikaros—japanese deep space solar sail demonstration mission," *Acta Astronautica*, vol. 82, no. 2, pp. 183–188, 2013.

[7] D. A. Spencer, B. Betts, J. M. Bellardo, A. Diaz, B. Plante, and J. R. Mansell, "The lightsail 2 solar sailing technology demonstration," *Advances in Space Research*, vol. 67, no. 9, pp. 2878–2889, 2021.

[8] J. R. Mansell, J. M. Bellardo, B. Betts, B. Plante, and D. A. Spencer, "Lightsail 2 solar sail control and orbit evolution," *Aerospace*, vol. 10, no. 7, p. 579, 2023.

[9] A. Farrés and À. Jorba, "A dynamical system approach for the station keeping of a solar sail," *The Journal of the Astronautical Sciences*, vol. 56, no. 2, pp. 199–230, 2008.

[10] J. Bookless and C. McInnes, "Control of lagrange point orbits using solar sail propulsion," *Acta Astronautica*, vol. 62, no. 2-3, pp. 159–176, 2008.

[11] A. Domahidi, E. Chu, and S. Boyd, "Ecos: An socp solver for embedded systems," in *2013 European control conference (ECC)*. IEEE, 2013, pp. 3071–3076.

[12] P. J. Goulart and Y. Chen, "Clarabel: An interior-point solver for conic programs with quadratic objectives," 2024.

[13] W. S. Koon, M. W. Lo, J. E. Marsden, and S. D. Ross, "Dynamical systems, the three-body problem and space mission design," in *Equadiff 99: (In 2 Volumes)*. World Scientific, 2000, pp. 1167–1181.

[14] S. P. Boyd and L. Vandenberghe, *Convex optimization*. Cambridge university press, 2004.

[15] I. Ross, "How to find minimum-fuel controllers," in *AIAA Guidance, Navigation, and Control Conference and Exhibit*, 2004, p. 5346.

[16] C. Acton, "Ancillary Data Services of NASA's Navigation and Ancillary Information Facility," *Planetary and Space Science*, vol. 44, no. 1, pp. 65–70, 1996.

[17] M. Udell, K. Mohan, D. Zeng, J. Hong, S. Diamond,

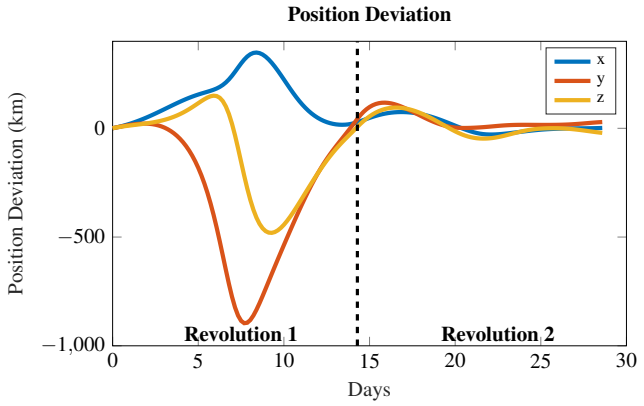

(a) Position deviation from the L2 halo orbit for two revolutions.

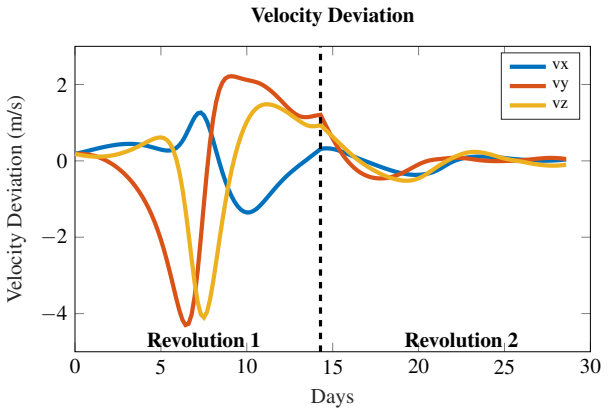

(b) Velocity deviation from the L2 halo orbit for two revolutions.

Figure 12: State deviation from the L2 halo orbit in the Earth-Moon system for Example 2. The dashed line represents the end of the first revolution.

and S. Boyd, "Convex optimization in julia," in *2014 First Workshop for High Performance Technical Computing in Dynamic Languages*. IEEE, 2014, pp. 18–28.

[18] J. Bezanson, S. Karpinski, V. B. Shah, and A. Edelman, "Julia: A fast dynamic language for technical computing," *arXiv preprint arXiv:1209.5145*, 2012.

[19] P. J. Goulart and Y. Chen, "Clarabel: An interior-point solver for conic programs with quadratic objectives," *arXiv preprint arXiv:2405.12762*, 2024.

[20] A. Wächter and L. T. Biegler, "On the implementation of an interior-point filter line-search algorithm for large-scale nonlinear programming," *Mathematical programming*, vol. 106, pp. 25–57, 2006.

[21] C. Rackauckas and Q. Nie, "DifferentialEquations.jl–a performant and feature-rich ecosystem for solving differential equations in Julia," *Journal of Open Research Software*, vol. 5, no. 1, 2017.

[22] E. Oland and R. Schlanbusch, "Reaction wheel design for cubesats," in *2009 4th International Conference on Recent Advances in Space Technologies*. IEEE, 2009, pp. 778–783.

[23] Jet Propulsion Laboratory. (2024) Periodic Orbits. NASA. [Online]. Available: https://ssd.jpl.nasa.gov/tools/periodic_orbits.html

BIOGRAPHY

Fausto Vega *is a PhD student at the Robotics Institute at Carnegie Mellon University (CMU). He received a BS in mechanical engineering from the University of Nevada, Las Vegas and an MS in Robotics at CMU. His research interests include small spacecraft state estimation and optimal control for maneuver design.*

Zac Manchester *is an assistant professor in the Robotics Institute at Carnegie Mellon University and founder of the Robotic Exploration Lab. He received a PhD in aerospace engineering in 2015 and a BS in applied physics in 2009, both from Cornell University. His research interests include control and optimization with applications to aerospace and robotic systems.*